ADVANCED FUNCTIONAL MATERIALS
www.afm-journal.de

Separation of Ultrahigh-Purity Long Semiconducting Carbon Nanotubes via Gel Chromatography

*Wenke Wang, Xiao Li, Chengjun Huang, Jiayi Xing, Linhai Li, Yanchun Wang, Xiaojun Wei, Haifang Yang, Weiya Zhou, and Huaping Liu**

Mass production of ultrahigh-purity long semiconducting single-wall carbon nanotubes (s-SWCNTs) is essential for their utilization in high-performance carbon-based devices. Here, the separation of ultrahigh-purity long s-SWCNTs is achieved by integrating repeated short-duration ultrasonic dispersion with iterative separation via gel chromatography. The resulting s-SWCNTs are confirmed to have a purity exceeding 99.9999%, representing the highest purity achieved via surfactant-based separation methods. Additionally, the average length of the separated s-SWCNTs exceeds 430 nm, with ≈47% surpassing 400 nm in length—more than twice the length of those obtained through traditional dispersion and separation methods. From these, a subset of s-SWCNTs with an average length of ≈674 nm and 79.8% exceeding 400 nm is further extracted for fabricating SWCNT thin-film transistors. The resulting transistors exhibit markedly superior transport performance compared to those derived from s-SWCNTs produced via conventional methods, characterized by significantly higher on-state conductance of ≈149 μS μm^{-1}, higher carrier mobility of over 89.1 cm^{2}V^{-1}s^{-1} and a high on/off ratio exceeding 10^5. The work demonstrates the exceptional separation capability of surfactant-based gel chromatography in producing ultrahigh-purity long s-SWCNTs with minimal defects, which holds significant promise for advancing the application of SWCNTs in high-performance electronic devices.

1. Introduction

Single-wall carbon nanotubes (SWCNTs) are regarded as ideal materials for fabricating high-speed, low-power electronic and optoelectronic devices owing to their exceptionally high carrier mobility,[1,2] superior gate control capability,[3,4] tunable energy gap,[5,6] and broad optical response spectrum.[7] Compared with traditional silicon-based devices at the same technology node, SWCNT-based devices exhibit an improvement in energy efficiency by over one order of magnitude.[8] Within the same device dimensions, the simulation results show that the performance of SWCNT devices surpasses that of silicon-based devices by one to two generations. For instance, the performance of 28 nm node SWCNT devices is comparable to that of 7 nm node silicon-based devices.[9] Further theoretical studies indicate that the energy efficiency of 3D integrated circuits based on SWCNTs could potentially exceed existing silicon-based circuits by a factor of 1000.[10] Consequently, the advancement of SWCNT-based devices represents a key direction for future device development.

SWCNTs can exhibit either metallic or semiconducting properties depending on their chirality. The cornerstone of constructing high-performance SWCNT-based integrated circuits (ICs) containing billions of transistors is the mass production of ultrahigh-purity semiconducting SWCNTs (s-SWCNTs), with a semiconducting purity exceeding 99.9999%.[11] This is because even trace amounts of metallic SWCNTs (m-SWCNTs) in the device channel can result in significant leakage currents and compromise the logical functionality of ICs. Currently, catalyzed growth methods are unable to synthesize ultrapure s-SWCNTs.[12–15] To achieve high-purity s-SWCNTs, various separation techniques have been developed, including density gradient ultracentrifugation (DGU),[16,17] DNA-encapsulated separation,[18,19] gel chromatography,[20–23] aqueous two-phase extraction (ATPE)[24–26] and polymer wrapping.[27–30] Among these methods, the conjugated polymer poly[9-(1-octylonoyl)-9H-carbazole-2,7-diyl] (PCz)-wrapped approach has proven effective in separating ultra-purity s-SWCNTs with a purity greater than 99.9999%.[31] However, this process requires the use of toxic and environmentally detrimental organic solvents such as toluene. Moreover, conjugated polymer molecules exhibit limited efficacy in recognizing the chiral structure of SWCNTs, making it challenging to separate single-chirality s-SWCNTs.[32] This limitation restricts the application of s-SWCNTs in

W. Wang, X. Li, C. Huang, J. Xing, L. Li, Y. Wang, X. Wei, H. Yang, W. Zhou, H. Liu
Beijing National Laboratory for Condensed Matter Physics
Institute of Physics
Chinese Academy of Sciences
Beijing 100190, China
E-mail: liuhuaping@iphy.ac.cn
W. Wang, X. Li, C. Huang, J. Xing, L. Li, X. Wei, W. Zhou, H. Liu
Center of Materials Science and Optoelectronics Engineering and school of Physical Sciences
University of Chinese Academy of Sciences
Beijing 100049, China
W. Wang, X. Li, C. Huang, J. Xing, L. Li, Y. Wang, X. Wei, W. Zhou, H. Liu
Beijing Key Laboratory for Advanced Functional Materials and Structure Research
Beijing 100190, China

DOI: 10.1002/adfm.202507593

high-performance carbon-based devices. Additionally, residual conjugated polymer molecules on the separated s-SWCNTs are difficult to remove due to their strong interaction with SWCNTs and high decomposition temperature,[33] which can degrade the electrical transport performance of SWCNT film. In contrast, surfactant-based separation techniques provide superior resolution in chirality, high separation efficiency, and cost-effectiveness.[34,35] Notably, gel chromatography has enabled milligram-scale separation of multiple single-chirality SWCNTs.[36,37] More importantly, residual surfactants around the separated SWCNTs can be readily removed.[38] Nevertheless, there have been no reports to date of achieving ultrapure s-SWCNTs with a semiconducting purity exceeding 99.9999% using surfactant-based methods.

The preparation of individualized SWCNT solution is a critical step in the separation of high-purity s-SWCNTs, directly influencing the semiconducting purity of the separated materials. Currently, ultrasonic dispersion is the most prevalent method for dispersing SWCNTs, where SWCNT bundles are dispersed into individual SWCNTs or smaller bundles through shear forces generated by acoustic cavitation.[39] To enhance the dispersion efficiency and yield of SWCNTs in aqueous solutions, extended ultrasonic treatment is often required. However, prolonged ultrasonic dispersion can lead to an increase in defects and a reduction in length, particularly for already dissociated individuals and small bundles,[40–44] which may degrade the carrier transport performance of SWCNTs in electronic devices.[45] Traditional ultrasonic dispersion techniques encounter significant challenges in simultaneously achieving long lengths with minimal defects and high dispersibility. Consequently, current surfactant-based separation methods typically produce s-SWCNTs and single-chirality species with average lengths shorter than 300 nm.[18,24,38,46,47] Such short lengths pose challenges in directly connecting the source and drain electrodes of transistor devices. This significantly restricts the fabrication of high-performance carbon-based devices.

To mitigate prolonged ultrasonic damage to the crystal structure of SWCNTs, we developed a protocol that integrates repeated short-duration 10 min ultrasonic dispersion of 30 W cm^{-2} with centrifugal extraction. This method enables the preparation of long SWCNT dispersions with minimal structural defects. Using this approach, the average length of dispersed SWCNTs exceeds 430 nm, with 47% exceeding 400 nm. Compared to conventional ultrasonic dispersion techniques, this method significantly reduces structural defects and doubles the average length of SWCNTs. However, due to the brief ultrasonication periods, some SWCNTs remain in small bundles, leading to the co-adsorption of m- and s-SWCNTs within the gel matrix medium, thereby reducing the purity of the separated s-SWCNTs. To achieve ultrahigh-purity s-SWCNTs, multiple iterative separations were conducted via gel chromatography. Prior to each separation, the previously separated s-SWCNTs were redispersed via low-power density of 6 W cm^{-2} and short-duration ultrasonication of 1 min per 20 mL to disperse residual small bundles. After five rounds of separation, optical spectroscopy and electrical characterization confirmed that the purity of the separated s-SWCNTs exceeded 99.9999%, representing the highest semiconducting purity achieved by surfactant-based separation methods to date. Additionally, their lengths remained unchanged compared to the initially dispersed SWCNTs. Long s-SWCNTs with an average length of 674 nm were further extracted from the separated s-SWCNTs for the fabrication of SWCNT network thin film transistors (SWCNT-TFTs). The on-state conductance of the resulting SWCNT-TFTs reached ≈149 μS $μm^{-1}$, and the carrier mobility exceeded 89.1 $cm^2V^{-1}s^{-1}$. These values are 3.7 times higher and 3.6 times higher, respectively, compared to those of devices derived from short s-SWCNTs prepared using traditional methods, while remaining a high on/off ratio of 10^5. These performance metrics also surpass those reported in previous studies on SWCNT network film transistors.[29,38,48–62] These results demonstrate that gel chromatography exhibits superior performance in the preparation of ultra-high purity, long SWCNTs with minimal structural defects, making it highly suitable for the development and application of high-performance carbon-based devices.

2. Results and Discussion

2.1. The Influence of the Ultrasonic Dispersion Duration on the Individual Yield, Defect Density, Length, and Dispersion Efficiency of SWCNTs

The dispersion of SWCNTs in aqueous solutions is an essential prerequisite for achieving the separation of high-purity s-SWCNTs via gel chromatography. While extending ultrasonic dispersion time can enhance SWCNT dispersion, it also leads to an increase in defects and shortening of the SWCNTs. To achieve a long SWCNT dispersion with minimal defects, we conducted a systematic investigation into the effects of ultrasonic dispersion time on the yield, defect density, length, and dispersion quality of arc-discharge synthesized SWCNTs (AD-SWCNTs). Sodium cholate (SC) surfactant, known for its strong interaction with SWCNTs,[63] was employed to enhance the dispersibility of SWCNTs. Specifically, 12 mg of AD-SWCNTs were dispersed in 20 mL aqueous solution of 0.5 wt % SC (99.0%, Sigma-Aldrich) using a tip ultrasonic homogenizer (Sonifire 450D, Branson) at a power density of 30 W cm^{-2}. The ultrasonic duration was varied from 5 min to 8 h. Following sonication, the SWCNT suspension was subjected to ultracentrifugation (S50A, CS150FNX, Hitachi) at 210 000 g for 1 h to remove the undispersed bundles, after which the upper 80% of the supernatant was collected as the SWCNT dispersion for further characterization. The inset in **Figure 1a** illustrates the optical absorption spectra of SWCNT dispersions obtained at different ultrasonic durations. It is evident that the optical absorbance of the prepared SWCNT dispersion increases with prolonged ultrasonic dispersion time, indicating enhanced dispersion efficiency. To quantify the concentration of SWCNT dispersion, the optical absorbance at 280 nm was measured and compared. As depicted in Figure 1a, the increase in optical absorbance can be categorized into three stages: during the first stage (5 min to 1 h), absorbance rises rapidly; in the second stage (1 to 3 h), the increase rate of absorbance slows down; and in the third stage (after 3 h), the optical absorbance reaches saturation over dispersion time.

The defects in the SWCNTs in dispersion obtained after varying ultrasonic duration were characterized by Raman spectroscopy at 532 nm excitation. As shown in Figures 1b and S1 (Supporting Information), the normalized Raman spectra at the G-band indicate that the intensity of the D-band increases with prolonged ultrasonic time, suggesting that extended ultrasonic

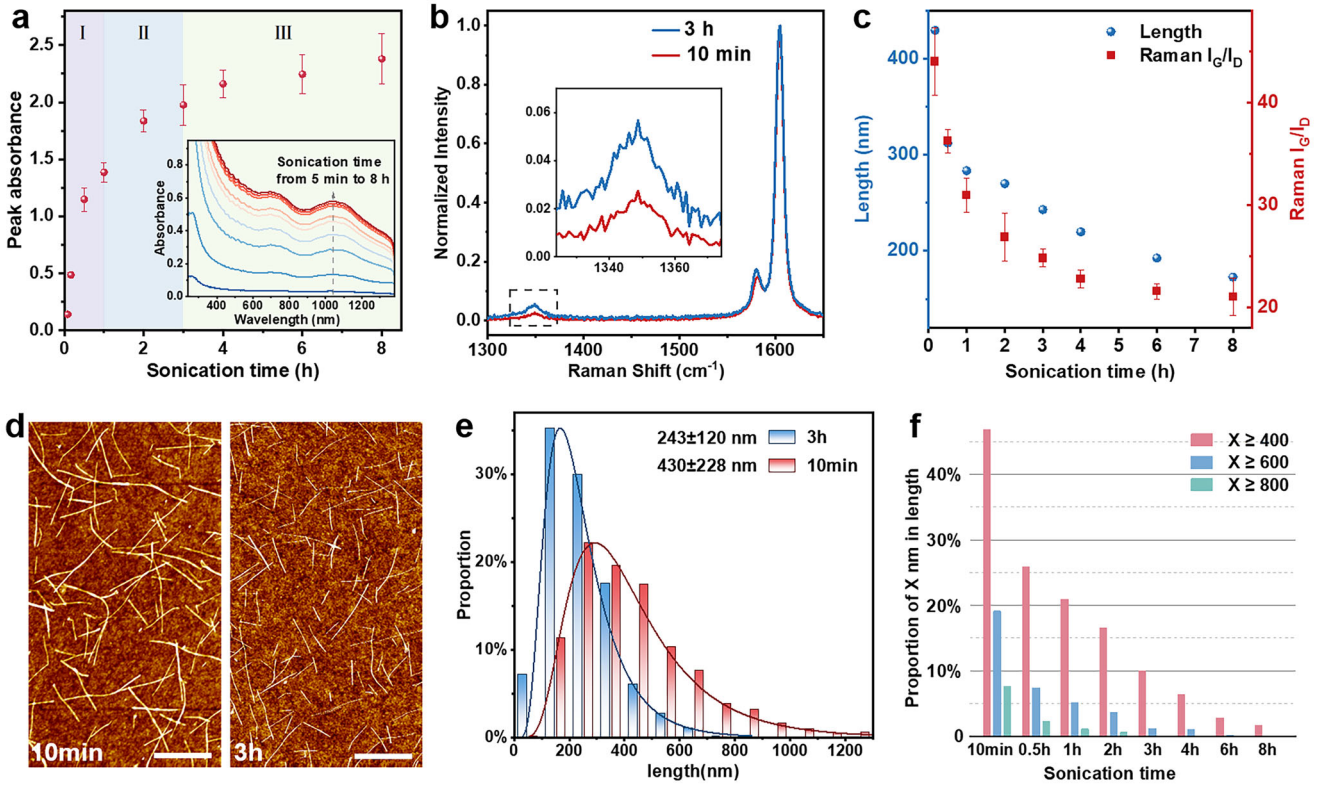

Figure 1. Influence of ultrasonication duration on the yield, defects, and length of dispersed SWCNTs. a) Variation in optical absorbance at 280 nm (after a 30 fold dilution) of as-dispersed SWCNT solutions as a function of sonication time. The inset provides the corresponding optical absorption spectra. b) Raman spectra (measured under 532 nm laser excitation) of sorted s-SWCNTs derived from SWCNT solutions prepared via ultrasonic dispersion for 10 min and 3 h, respectively, normalized with respect to the G-band intensity. The inset provides an enlarged view of the D-band region. c) Variation in the average length and defect density of SWCNTs, as characterized by the G-to-D intensity ratio from Raman spectroscopy, with respect to ultrasonic dispersion duration. d) AFM images of s-SWCNT films separated from SWCNT solution after ultrasonic dispersion for 10 min and 3 h, respectively. The scale bars in AFM are 500 nm. e) The statistical length distribution of the separated s-SWCNTs is presented in Figure D. f) Variation in the proportion of s-SWCNTs exceeding X nm in length (where X = 400, 600, and 800 nm) separated from the SWCNT solutions following ultrasonic dispersion for varying durations.

treatment introduces more defects into the SWCNTs. To quantify the increased trend of the defect density introduced by ultrasonication, the relationship between the G/D ratios of the Raman spectra and ultrasonic time is depicted in Figure 1c. The G/D ratio decreases rapidly from 44 to 31 as the ultrasonic time increases from 10 min to 1 h. After 1 h of ultrasonication, the rate of decrease in the G/D ratio slows down over dispersion time, and after 4 h of ultrasonication, the G/D ratio of the dispersed SWCNTs shows only a slight further reduction with an increase in ultrasonic time. This suggests that the majority of defects are introduced within the first h of ultrasonic dispersion.

For SWCNT-based FETs, the transport processes of carriers are commonly modeled using a percolation approach.[64–66] Longer SWCNTs exhibit a higher probability of bridging the source and drain electrodes, thereby significantly enhancing carrier transport efficiency and improving device performance. For this, we systematically investigated the impact of ultrasonic dispersion duration on the length reduction of SWCNTs using atomic force microscopy (AFM). The dispersed SWCNTs were deposited on SiO_2/Si substrates via the small molecule tuning method previously reported by our research group.[67] As illustrated in Figures 1d and S2 and S3 (Supporting Information), increasing ultrasonication duration causes a decrease in the length of SWCNTs. Statistical analysis reveals that the average length of SWCNTs decreases from ≈430 nm with ≈50% shorter than 400 nm after 10 min of ultrasonic dispersion to ≈243 nm with ≈90% being shorter than 400 nm after 3 h (Figure 1c–f). As the ultrasonication duration further prolonged to 8 h, the average length of SWCNTs is reduced to 173 nm (Figure 1c). Notably, the average length decreases rapidly within the first h of ultrasonic dispersion, with the shortening rate gradually slowing down thereafter, consistent with the increase in defects. To further explore the influence of ultrasonic dispersion on the shortening effect of SWCNTs, we conducted a statistical analysis of the trend in the proportion of different SWCNT lengths over dispersion time. As depicted in Figure 1f, SWCNTs longer than 800 nm shorten more rapidly and disappear after 3 h of ultrasonic dispersion. SWCNTs longer than 600 nm vanish after 4 h while those longer than 400 nm only account for ≈2.8%. These findings indicate that longer SWCNTs are more susceptible to fragmentation under ultrasonic dispersion.

The effects of ultrasonication on SWCNTs can be categorized into two principal aspects: first, the exfoliation of individual or small bundles of SWCNTs from larger bundles; and second, the fragmentation of these isolated single or small bundle

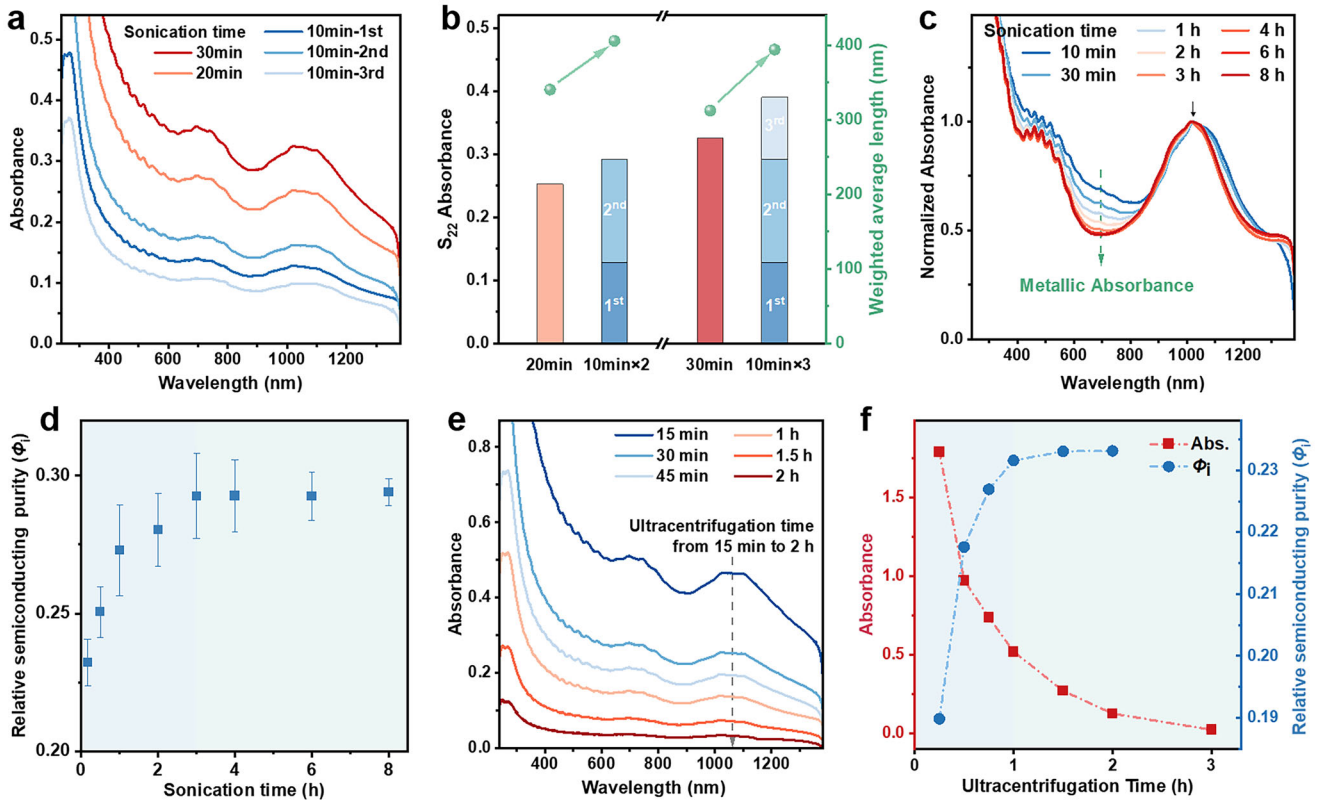

Figure 2. Impact of ultrasonic dispersion duration and ultracentrifugation time on the dispersion efficiency of SWCNTs. a) Optical absorption spectra were obtained from SWCNT solutions that were diluted 30 fold following continuous ultrasonic dispersion for durations of 20 and 30 min, as well as multiple 10 min cyclic ultrasonic dispersions. b) Stacked column charts of the absorbance at 1015 nm in the S_{22} region in Figure (a). Green dots signify the corresponding weighted average lengths, with the calculation methodology detailed in the supporting information (Note S1, Supporting Information). c) Optical absorption spectra (normalized to the maximum absorbance in the S_{22} region) of s-SWCNTs, separated from SWCNT solutions following different continuous dispersion durations. d) The trend of relative semiconducting purity, as evaluated by the Φ_i value, of s-SWCNTs separated from SWCNT solutions with varying continuous dispersion times, which was calculated based on the optical absorption spectra presented in Figures 2c and S6 (Supporting Information). For detailed calculation methods, please refer to Note S2 (Supporting Information) in the supplementary information. e) Optical absorption spectra of the supernatant (diluted 30 times) from SWCNT solutions, which were ultrasonically dispersed for 10 min and subsequently subjected to varying centrifugation times. f) The optical absorbance at 280 nm in the optical absorption spectra in (e), as well as the relative purity (Φ_i) of the separated s-SWCNTs as a function of ultracentrifugation time.

SWCNTs into shorter segments due to defects caused by continuous intense ultrasonic cavitation. Continuous ultrasonic dispersion progressively exfoliates and disperses an increasing number of individual and small bundles of SWCNTs in the solution, leading to a rapid increase in their concentration. This increased concentration consumes more ultrasonic power, thereby gradually reducing the efficiency of exfoliating individual SWCNTs from large bundles. Consequently, the concentration of dispersed SWCNTs approaches saturation (Figure 1a). Simultaneously, as the concentration of individual and small bundle SWCNTs rises, the probability of buckling or stretching-induced breakages due to cavitation increases, particularly for longer SWCNTs,[43,44] resulting in their fragmentation into shorter segments. Although these processes occur concurrently, from a reaction kinetics standpoint, we can leverage differences in their reaction rates to minimize damage and obtain long SWCNTs with few defects by reducing ultrasonic dispersion time.

To minimize the damage to the exfoliated individuals or small SWCNT bundles during continuous ultrasonic dispersion, we developed a protocol that integrates repeated short-duration ultrasonic dispersion with centrifugal extraction. Specifically, SWCNTs were subjected to ultrasonic dispersion at a power density of 30 W cm^{-2} for 10 min, followed by centrifugation to extract the supernatant of 80%. An equal volume of surfactant aqueous solution was added, and the mixture was redispersed for another 10 min. This process was repeated three times. **Figure 2a** shows the absorption spectra of three SWCNT solutions after three 10 min dispersion cycles. For comparison, the absorption spectra of the SWCNT solution obtained by continuous 20 and 30 min ultrasonic dispersion are presented. Compared with the SWCNT dispersion obtained from a continuous 20 min ultrasonic treatment, the cumulative optical absorbance at 1015 nm of SWCNT solutions obtained by two 10 min dispersion cycles is significantly higher, indicating more efficient dispersion of nanotubes. More importantly, the weighted average length of SWCNTs is ≈405 nm, which is ≈65 nm longer than that of SWCNTs dispersed continuously for 20 min, as shown in Figure 2b (see detailed methodology in Note S1 and Figure S4, Supporting Information). Similarly, the cumulative optical absorbance at 1015 nm of SWCNTs solutions obtained by three 10 min dispersion cycles is greater

than that of the SWCNT solution obtained from a continuous 30 min ultrasonic treatment. Statistical analysis reveals that the weighted average length of the SWCNTs is ≈394 nm, which is ≈82 nm longer than that of nanotubes dispersed continuously for 30 min. Clearly, prolonged ultrasonic dispersion primarily shortens SWCNTs through shear-induced damage to individual and small bundles of nanotubes that have been exfoliated. Therefore, repeated short-duration ultrasonic dispersion not only enhances the dispersion yield of individualized SWCNTs but also minimizes the damage and potential shortening caused by continuous ultrasonic treatment.

As previously discussed, the dispersion degree of SWCNTs significantly influences the purity of the separated s-SWCNTs. Gel chromatography separates s-SWCNTs primarily through their selective adsorption within the gel matrix. This process is controlled by the density or coverage of surfactant molecules on their surfaces.[34,35] Specifically, the higher the density or coverage of surfactant molecules on SWCNTs, the weaker the interaction between SWCNTs and the gel matrix becomes. M-SWCNTs, due to their relatively low redox potential, are susceptible to oxidation and carry a positive charge in oxygen-rich aqueous solutions.[22,23,25] This characteristic facilitates stronger adsorption of anionic surfactant molecules onto m-SWCNTs, resulting in a higher density of surfactant molecules surrounding them.[22] Consequently, at a given surfactant concentration, m-SWCNTs exhibit relatively weak adsorption affinity within the gel medium. In contrast, s-SWCNTs, which have a lower density of surfactant molecules, demonstrate stronger adsorption affinity within the gel matrix. Therefore, upon loading the dispersed SWCNT solution into the gel column, s-SWCNTs are adsorbed onto the gel column while m-SWCNTs pass directly through the gel column. In this manner, the separation of m-/s-SWCNTs can be achieved. However, inadequate dispersion would result in the presence of SWCNT bundles containing both m- and s-SWCNTs in the SWCNT dispersion. These bundles can be adsorbed onto the gel medium after loading SWCNT dispersion into a gel column, thereby reducing the purity of the separated s-SWCNTs. To evaluate the impact of different dispersion durations on SWCNT dispersion, we conducted a series of separations using gel chromatography. Prior to the separation experiment, the concentration of SC in SWCNT dispersion was decreased from 0.5 to 0.1 wt % to improve the affinity between s-SWCNTs and gel media. Simultaneously, sodium dodecyl sulfate (SDS) with a concentration of 0.6 wt % was introduced to partially replace the SC adsorbed on the SWCNTs, thereby exposing a greater surface area of the s-SWCNTs.[36] The results of three independent separation experiments for each dispersion time are presented in Figures 2c and S5 (Supporting Information). As ultrasonic dispersion time increased, the optical absorption peaks associated with m-SWCNTs gradually diminished, suggesting enhanced purity of the separated s-SWCNTs. To quantify this effect, the relative semiconducting purity (Φ_i) of the sorted s-SWCNTs was calculated from optical absorption spectra (refer to Note S2 and Figure S6 for detailed methodology, and Supporting Information). The results are shown in Figure 2d and Table S1 (Supporting Information). The standard deviations of three replicate experiments are presented as error bars. The coefficient of variation (CV) for each set of replicate experiments was calculated by dividing the standard deviation by the mean. The results indicate that the CV for all replicate experiments is less than 6.1%, which demonstrates the high reproducibility of the experimental findings. Higher Φ_i values correspond to greater purity.[68] As dispersion time increased from 10 min to 1 h, there was a rapid increase in purity. After that, the purity increased slowly. After 3 h, further increases in dispersion time did not significantly affect the Φ_i value, indicating minimal changes in purity, consistent with the observed trends in dispersion yield. Clearly, short ultrasonic dispersion time was insufficient to fully disperse small-bundle SWCNTs.

Alternatively, to achieve high-purity s-SWCNTs from 10-min ultrasonically dispersed SWCNTs, the concentration of small SWCNT bundles in the dispersion solution can be reduced by extending ultracentrifugation time. To validate this approach, we investigated the impact of ultracentrifugation duration on the purity of separated s-SWCNTs. As illustrated in Figure 2e,f, increasing the ultracentrifugation time from 15 min to 2 h resulted in a significant decrease in the absorbance of the pristine SWCNT solutions, leading to yield loss. S-SWCNTs were separated from the SWCNT solutions subjected to varying ultracentrifugation durations. The corresponding optical absorption spectra are presented in Figure S7 (Supporting Information). The relative semiconducting purities (Φ_i) were calculated. As shown in Figure 2f, the relative purity of the sorted s-SWCNTs increased markedly within the first h of ultracentrifugation. Beyond this point, further improvements in purity became marginal, while the concentration of pristine SWCNT solutions continued to decline until it reached zero. Notably, despite undergoing ultracentrifugation for two h, the absorption peak of m-SWCNTs remains clearly visible in the absorption spectrum of the separated s-SWCNTs. At this point, the recovery rate of dispersed SWCNTs is less than a quarter of that with one-h ultracentrifugation. This suggests that simply increasing the duration of centrifugation to remove SWCNT bundles is not an effective method for enhancing the purity of the separated s-SWCNTs.

To ensure the effective recovery and dispersion of SWCNTs, repeated ultrasonic dispersion of the recovered supernatant solution is proposed as an alternative method (**Figure 3a**). Given that only small bundles of SWCNTs are present in the recovered supernatant, low-power ultrasonic treatment can effectively disperse these bundles into individual tubes while minimizing damage to their crystalline structure.[41,42] Specifically, a low ultrasonic power density of 6 W cm^{-2} and a short dispersion time (1 min per 20 mL) were employed for redispersion to minimize damage to the crystalline structure of SWCNTs. Subsequently, the separation of s-SWCNTs was conducted to evaluate the dispersion quality, as illustrated in the blue experimental flow of Figure 3a. The optical absorption spectra show a significant reduction in absorption peaks for m-SWCNTs compared to that of the s-SWCNTs separated from the initial SWCNT dispersion (the black experimental flow in Figure 3a), indicating a marked improvement in the semiconducting purity of the sorted s-SWCNTs (Figure 3b,c). Moreover, AFM images (Figure S8, Supporting Information) confirm that the length of SWCNTs has not been compromised. Based on these findings, we propose that repeated short-duration, low-power ultrasonic dispersion combined with iterative separation by gel chromatography may facilitate the production of ultrahigh-purity long s-SWCNTs, as illustrated in the red experimental flow of Figure 3a.

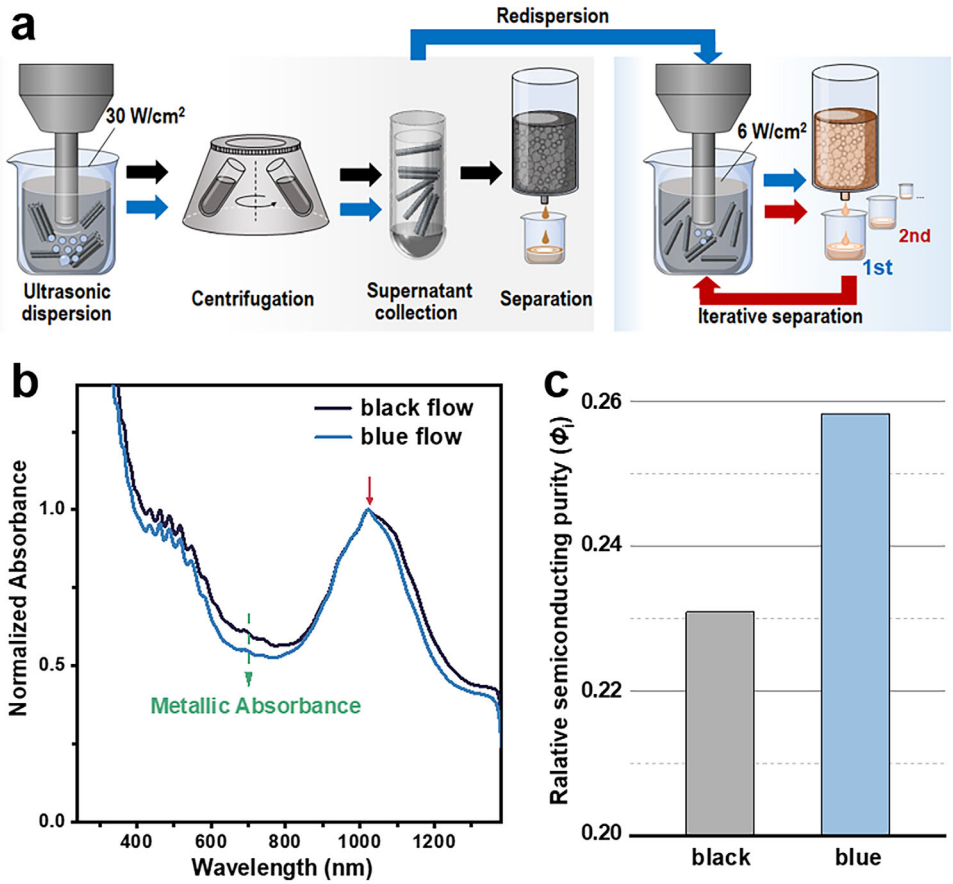

Figure 3. Impact of low-power ultrasonic redispersion on the dispersibility of SWCNTs. a) Schematic diagram of strategy for low-power ultrasonic redispersion and evaluation of dispersion efficiency and semiconducting purity of SWCNTs. b) Optical absorption spectra of the separated s-SWCNTs obtained from the black and blue experimental flows in (a). The spectra are normalized by the maximum of S_{22} absorbance. c) The relative purity (assessed by Φ_i value) of the sorted s-SWCNTs in (b).

2.2. The Separation of Ultrahigh-Purity Long Semiconducting SWCNTs

To produce ultra-high purity long s-SWCNTs, we have extended the blue route separation method by an iterative combination of low-power, short-duration ultrasonic dispersion and gel chromatography separation (as depicted in the red experimental flow in Figure 3a). **Figure** 4a illustrates the normalized optical absorption spectra of the separated s-SWCNT solutions (refer to Figure S9, Supporting Information for additional details). As the number of separation cycles increased, the valley in the 600–800 nm region, corresponding to the optical absorption of m-SWCNTs, deepened, indicating enhanced semiconducting purity. Additionally, the absorption peak in the 800–1200 nm range, associated with the S_{22} transition, exhibited a blue shift, suggesting a reduction in the average diameter of the s-SWCNTs. Compared to smaller-diameter s-SWCNTs, larger-diameter s-SWCNTs exhibit a relatively lower redox potential and demonstrate stronger interactions with anionic surfactants.[22] Consequently, a higher density of surfactants is adsorbed onto their surfaces, leading to weaker adsorption affinities with the gel matrix. Insufficient dispersion results in the presence of bundles containing both large- and small-diameter s-SWCNTs, which causes co-adsorption with smaller-diameter counterparts in the gel column. Enhanced dispersibility reduces the adsorption probability of individual larger-diameter s-SWCNTs within the gel medium, ultimately resulting in a decrease in the average diameter of the separated s-SWCNTs.

With the increase in the number of repeated separation cycles, the absorption peak corresponding to m-SWCNTs gradually diminished, surpassing the detection limit for m-SWCNTs using optical absorption spectroscopy. Raman spectroscopy exhibits superior sensitivity to m-SWCNTs due to resonance excitation effects and was employed to further characterize the purity of the separated s-SWCNTs after each separation cycle. Figure 4b presents the Raman spectra of the separated s-SWCNTs, excited at wavelengths 532, 633, and 785 nm, normalized relative to the absorption peak at 280 nm in the optical absorption spectra. The signal intensity of m-SWCNTs decreases progressively with an increase in the number of separation cycles. Following five rounds of separation, no traces of m-SWCNTs can be detected, indicating the attainment of high-purity s-SWCNTs. These results are consistent with their optical absorption spectra.

Due to the introduction of low-power ultrasonic dispersion prior to each separation cycle, it was necessary to verify whether weak ultrasonic dispersion leads to an increase in defects and a shortening effect on SWCNTs. To this end, Raman spectroscopy

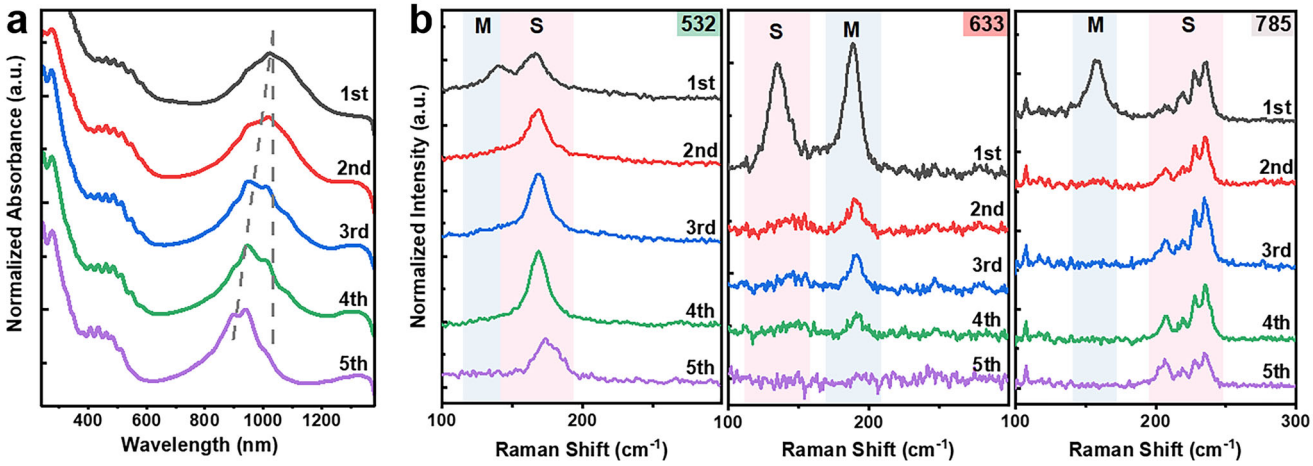

Figure 4. Spectral characterization of s-SWCNTs obtained through iterative separation. a) Optical absorption spectra of the sorted s-SWCNTs following each round of iterative separations. The spectra have been normalized to the maximum absorbance in the S_{22} region and vertically offset for comparative analysis. b) Raman spectra of the sorted s-SWCNTs after each round of iterative separations, normalized relative to the absorbance at 280 nm from the corresponding optical absorption spectra shown in Figures 4a and S8 (Supporting Information) and vertically offset for comparative analysis. The Raman spectra, measured under 532, 633, and 785 nm laser excitation (from left to right), are presented with wavenumber ranges for metallic and semiconducting signals highlighted in different colors according to the Kataura plot.[69,70]

and AFM were utilized to characterize the defect levels and length distribution of the separated s-SWCNTs. As illustrated in **Figure** 5a, when normalizing the Raman spectra by the G-band, the relative intensity of the D-band remains constant across increasing rounds of separations, indicating that the sorted s-SWCNTs maintain a consistently low defect level. Figure 5b presents the length distribution of the sorted s-SWCNTs after multiple rounds of separations (refer to Figure S10, Supporting Information for more details, and supporting information). The average lengths are consistently maintained at ≈430 nm. However, there is a slight decrease in the proportion of short SWCNTs, which should result from losses of irreversible adsorption within the gel column.[51] Notably, even after five rounds of iterative separations, the proportion of SWCNTs longer than 400 nm exceeds 46.8%, which facilitates the fabrication of high-performance devices.

Despite the inability to detect m-SWCNTs via optical absorption spectra and Raman spectra after five rounds of separation, the precise purity of the separated s-SWCNTs remains undetermined. To quantitatively assess the purity of the separated s-SWCNTs following five rounds of separation, back-gated thin-film transistors (TFTs) with simplified structures were fabricated on a SiO_2/Si substrate for measuring device transfer curves. In these devices, a 100-nm thick SiO_2 layer served as the dielectric layer, while heavily doped silicon functioned as gate electrodes. The schematic diagram of the TFT structure is

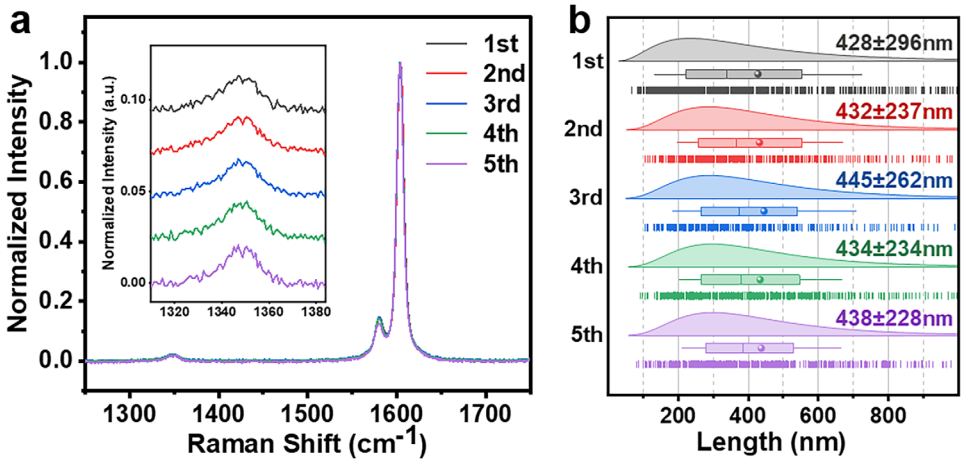

Figure 5. Characterization of defect density and length distribution of s-SWCNTs obtained through iterative separations. a) Raman spectra (measured under 532 nm laser excitation) of the sorted s-SWCNTs after each round of iterative separations, normalized by the G-band. The inset provides an enlarged view of the D-band region, with vertical offsets applied for comparative analysis. b) Length distribution of the sorted s-SWCNTs after each round of iterative separations. The boxes depict the first, second, and third quartiles of the length statistics, while the whiskers indicate the standard deviation. The dots within the boxes represent the average length. The curves above the boxes are fitted representations of the length distribution.

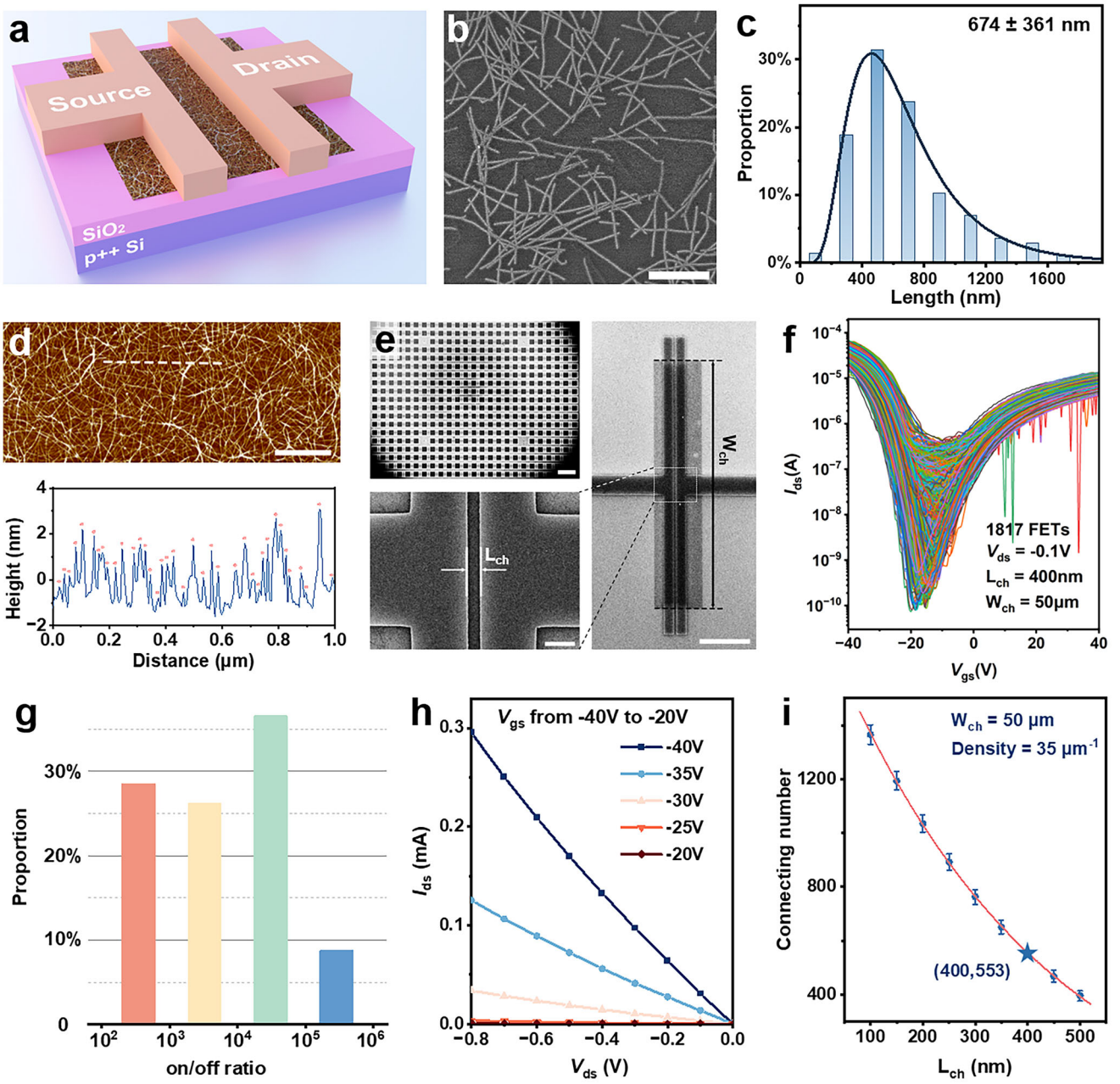

Figure 6. Evaluation of the semiconducting purity of the separated s-SWCNTs by electrical transport performances. a) Schematic diagram of the structure of back-gated TFTs. b) A typical SEM image and c) length distribution of s-SWCNTs were obtained after five rounds of iterative separation and subsequent length separation, where the scale bar is 800 nm. d) AFM image of the SWCNT network film used for TFT fabrication (the upper panel), where the scale bar is 500 nm. The lower panel is the height line profile corresponding to the dashed line in the AFM image, illustrating the linear density. e) SEM images of device arrays (top left), single device (right), and channel area (bottom left). The corresponding scale bars are 200 μm, 10 μm, and 1 μm, respectively. The channel length is 400 nm and the channel width is 50 μm. f) Transfer curves and g) on/off ratio distribution of the fabricated 1817 TFTs ($|V_{ds}|$ = 0.1 V). h) Typical output curves of the fabricated back-gated TFTs, with V_{gs} varying from -40 to -20 V in steps of 5 V. i) Number of SWCNTs directly connecting the source and drain electrodes for the devices with different channel lengths, as obtained by Monte Carlo simulations (refer to Note S3, Supporting Information). The red line represents a fit based on the simulated data points.

illustrated in **Figure** 6a (refer to the experimental section for details). Herein, the semiconducting purity of SWCNTs can be evaluated by determining the proportion of m-SWCNTs within the SWCNT films bridging the source and drain electrodes. To facilitate more SWCNTs bridging the source and drain electrodes, short-channel TFTs featuring a 400 nm channel length and a 50 μm channel width were defined. Additionally, long s-SWCNTs were extracted using the surfactant micelle-driven method.[71] As depicted in Figure 6b,c, the average length of the length-sorted SWCNTs reached ≈674 nm, which is ≈250 nm longer than

pre-separation lengths. Notably, 79.8% of the s-SWCNTs were longer than 400 nm, while ≈15.8% surpassed 1 μm in length, with a small fraction reaching lengths approaching 2 μm (Figure S11, Supporting Information). Prior to TFT construction, a high-density s-SWCNT film with a linear density of ≈35 tubes/μm was deposited on a Si/SiO_2 substrate via the immersion method, as shown in Figure 6d. To prevent the adverse effects of surfactant residues on the electrical performance of s-SWCNTs, thermal treatment, and rinsing procedures were conducted to remove surfactant molecules (for detailed procedures, see the experimental section).[38] As illustrated in Figure S12 (Supporting Information), following the application of thermal treatment and rinsing processes, no significant surfactant residue was detected on the surface of s-SWCNTs. Figures 6e and S13 (Supporting Information) present the SEM images of the fabricated TFT array and individual TFTs. A total of 1817 devices were fabricated, with their transfer curves illustrated in Figure 6f. The distribution of switching performance, based on the on/off ratio, is depicted in Figure 6g. All devices exhibit an on/off ratio exceeding 10^2 in the transfer curves, indicating that no m-SWCNTs directly bridge the source and drain electrodes. More comprehensive statistical analyses regarding device-to-device variations in the on/off ratio, on-state current, and carrier mobility are provided in Figure S14 (Supporting Information). It is clearly demonstrated that these devices possess an average on/off current ratio of $\approx 2.9 \times 10^4$, an average on-state current of roughly 30 μA, and a mean carrier mobility of ≈10 $cm^2V^{-1}s^{-1}$. Typical output curves in Figure 6h demonstrate a linear relationship between I_{ds} and $V_{ds,}$ suggesting excellent ohmic contact between the SWCNT film and metal electrodes. Given the random orientation of SWCNTs within the network film, it is challenging to ascertain the number of SWCNTs bridging the source and drain electrodes. To address this, we performed a Monte Carlo simulation based on the percolation model, accounting for the random orientation and specific length distribution of SWCNTs (see detailed methodology in Note S3, Figures S15 and S16, Supporting Information). As shown in Figure 6i, ≈553 nanotubes are directly connected to the source and drain electrodes in each device channel. Among the 1817 devices, ≈1004801 SWCNTs were measured, indicating that the purity of the sorted s-SWCNTs exceeds 99.9999%.

Although ultrahigh-purity s-SWCNTs are obtained through five rounds of separation, the simplicity and scalability of gel chromatography render it a promising technique for industrial-scale separation. As presented in Table S3 (Supporting Information), ≈96 mg of raw SWCNTs were dispersed in 720 mL solution. After conducting one separation experiment using a 70 mL gel column, ≈280 mL of ultrahigh-purity s-SWCNT solution was obtained, as depicted in Figure S17 (Supporting Information). By analyzing the relationship between the optical absorption spectrum and concentration,[72] the yield of ultrahigh purity s-SWCNTs was calculated to be ≈3.1 mg. This quantity is sufficient to fabricate over 660 pieces of 4-inch wafer films (see detailed calculation methods in Note S4, Supporting Information).

However, from a commercial standpoint, as the number of separation cycles increases, while the purity of the separated s-SWCNTs improves, there is a corresponding increase in processing time, material consumption, and energy expenditure, leading to an increase in separation costs. To clarify this, we conducted a detailed calculation of the purity, yield, processing time, and cost associated with the separation of s-SWCNTs in each cycle. The calculation of separation costs encompasses raw materials, operating materials, electricity, equipment depreciation and maintenance, labor, and other related expenses (for detailed calculation methods, refer to Tables S4–S6, Note S4, Supporting Information). The results are summarized in Table S7 (Supporting Information). As the number of separation cycles increases, the separation yield of s-SWCNTs decreases and the separation cost rises. Even so, the separation cost for the ultrahigh purity s-SWCNTs ultimately obtained is merely US$118 /mg. Due to the lack of data on the separation costs of other advanced separation methods such as DGU and polymer wrapping methods,[16,17,27–30] a comprehensive comparison cannot currently be conducted. For reference, we compared the separation cost of our method with the market prices of s-SWCNTs separated by these two methods.[73,74] As shown in **Table 1**, even with a small experimental separation scale, the separation cost of our method is only about one-ninth of the price of s-SWCNTs purified by the DGU method despite both methods relying on surfactant-based separation principles. Moreover, the semiconducting purity of the s-SWCNTs separated by the DGU is ≈99.9%, which is lower than that of our product. Compared with the commercially available s-SWCNTs separated by polymer wrapping method, the separation cost in our present work is only about half of their market price.

It is worth emphasizing that metallic SWCNTs, which could potentially be utilized for conductive films and were obtained during the separation of s-SWCNTs, were not taken into account in this study. Furthermore, low-purity s-SWCNTs generated as by-products during the separation process can potentially be reused to produce ultrahigh-purity s-SWCNTs through repeated separations (Figure S9, Supporting Information). Consequently, the actual separation cost of ultrahigh-purity s-SWCNTs can be partially offset by the economic value of the separated metallic SWCNTs and low-purity s-SWCNTs. Additionally, within a laboratory setting, gel columns can be scaled up to the liter level,[37] indicating that the separation yield of ultrahigh-purity s-SWCNTs could increase significantly, thereby leading to a substantial reduction in separation costs. These comparisons clearly demonstrate the advantages of our current separation technique for ultrahigh-purity s-SWCNTs.

Beyond cost considerations, we conducted an analysis of the environmental impact of our separation technique for producing ultrapure s-SWCNTs using a model that integrates life cycle assessment and techno-economic analysis based on the inventory data of the separation process of s-SWCNTs (see detailed methodology in Note S4, Supporting Information).[37,75] The results demonstrate that producing 1 mg of ultrahigh-purity s-SWCNTs with our technique generates ≈4.27 kg of CO_2 emissions. Therefore, the environmental impact of our current technique for ultrapure s-SWCNTs is relatively minimal. Consequently, our current separation technique holds significant potential for industrial application.

Table 1. Comparison of s-SWCNTs from different sources.

s-SWCNTs	Price & Cost	Method	Purity
Commercial product I[73]	US$1050 /mg	DGU	>99.9%
Commercial product II[74]	US$229 /mg	Polymer wrapping	>99.9999%
This technique	US$118 /mg	Gel Chromatography	>99.9999%

2.3. High-Performance Top-Gated TFTs Based on the Sorted Long s-SWCNTs

The separation of ultrahigh-purity long s-SWCNTs with minimal defects is undoubtedly advantageous for the development of high-performance TFTs. To validate this hypothesis, top-gated TFTs were constructed with a channel length of 400 nm and a channel width of 3.5 µm, as illustrated in the upper panel of **Figure** 7a. SWCNT films with a linear density of 30 tubes/µm were used as channel material. The typical morphology of the s-SWCNT film is presented in the lower panel of Figure 7a. The optical image of the devices and the false-colored SEM image of the channel region are shown in Figure 7b,c, respectively. Figure 7d,e illustrates the representative output and transfer curves. For comparative analysis, TFTs were also fabricated using short s-SWCNTs with an average length of 243 nm. These nanotubes underwent continuous dispersion for 3 h prior to separation. The corresponding output and transfer curves are also presented in Figure 7d,e. It is evident that the TFTs constructed with long s-SWCNTs exhibit significantly higher on-state currents. Their output curves demonstrate superior linearity under source-drain bias, indicating that the ultrahigh-purity long s-SWCNT film forms enhanced ohmic contacts with the metal electrodes. To further quantitatively evaluate the performance of both types of devices, key characteristics including on-state current, on-state conductance, carrier mobility, and on/off ratio were extracted (see detailed methodology in Note S5 and Figure S18, Supporting Information). As shown in Figures 7f and S19 (Supporting Information), the on-state current (I_{on}), maximum transconductance (g_m), and mobility of the long s-SWCNT TFTs reach 14.9 µA µm^{-1}, 11.1 µS µm^{-1}, and 89.1 cm^{2}V^{-1}s^{-1}, respectively. These values are 3.7, 3.6, and 3.6 times higher than those of the short s-SWCNT

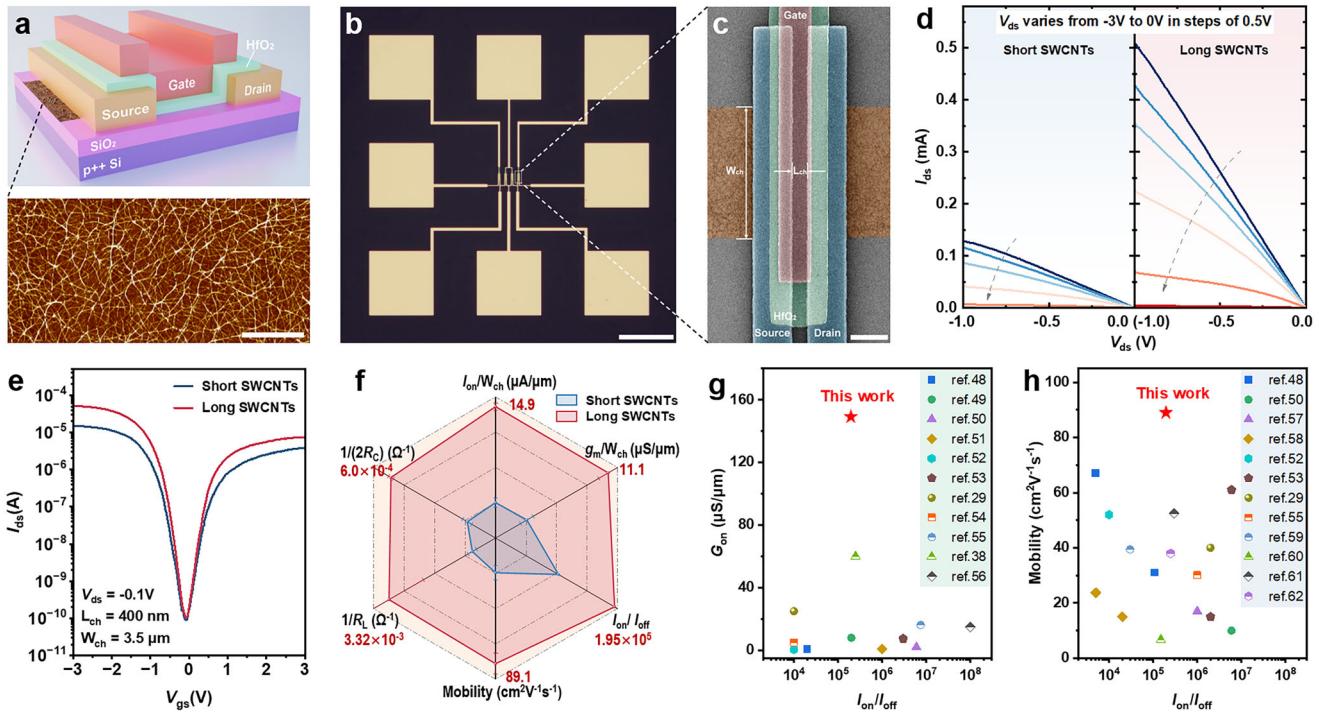

Figure 7. Characterization of the electrical transport performance of top-gated TFTs based on separated ultrahigh purity long s-SWCNTs. a) Schematic diagram (top) illustrating the structure of top-gated TFTs and AFM image (bottom) of the SWCNT network film utilized for TFT fabrication. The scale bar is 500 nm. b) Optical microscope image of the fabricated top-gated TFTs, with a scale bar of 50 µm. c) False-colored SEM image of the channel area, characterized by a length of 400 nm and a width of 3.5 µm. The scale bar is 1 µm. d) Representative output curves of the fabricated TFTs based on long and short s-SWCNT films, where V_{gs} varies from −3 to 0 V in increments of 0.5 V. e) Representative transfer curves of the fabricated TFTs based on long and short s-SWCNT films at $|V_{ds}| = 0.1$ V. f) Radar chart comparing six performance metrics (on-state current, transconductance, on/off ratio, mobility, channel resistance and contact resistance) between long and short s-SWCNT TFTs. g) Comparison of on-state conductance and on/off ratio of TFTs constructed from ultrahigh-purity long s-SWCNTs relative to previously reported network TFTs. h) Comparison of mobility and on/off ratio of TFTs constructed from ultrahigh-purity long s-SWCNTs with those of previously reported TFTs.

devices while maintaining superior switching performance with an on/off ratio exceeding 10^5. These performance metrics, especially on-state current and mobility, position the TFTs constructed from ultrahigh purity and long s-SWCNTs among the leading SWCNT network TFTs reported in previous studies (Figure 7g,h). To facilitate a direct comparison with previously reported device performance metrics, the on-state current is herein characterized by the on-state conductance (G_{on}) (Figure 7g), which is defined as the ratio of the on-state current to the source-drain bias voltage.

The superior electrical transport performance of transistors fabricated from ultra-purity long s-SWCNT films should be attributed to their long lengths and minimal defect density. These characteristics result in a significant reduction in channel resistance (R_L) and contact resistance (R_C) between the SWCNT film and metal electrodes. To validate this hypothesis, we performed comprehensive analyses of R_L and R_C for the long and short s-SWCNT devices. The results demonstrate that a long s-SWCNT TFT exhibits a 78% reduction in R_L and a 73% reduction in R_C compared to its short s-SWCNT counterpart, as illustrated in Figures 7f and S14 (Supporting Information). The decrease in R_L is primarily due to the sufficient length of the sorted s-SWCNTs, which effectively bridge the source and drain electrodes, thereby significantly reducing junction resistance for carrier transport between nanotubes.[76,77] Additionally, the lower defect level within the SWCNTs reduces the scattering probability of carriers, enhancing ballistic transport performance.[78,79] The reduction in R_C should be attributed to the decreased proportion of short s-SWCNTs that are in contact with the electrodes but do not form effective current pathways.[62] Consequently, TFTs based on these ultrahigh-purity, long, and low-defect s-SWCNTs exhibit markedly improved transport performances. These findings unequivocally highlight the capability of gel chromatography in preparing high-quality long s-SWCNTs, thereby providing a crucial material foundation for advancing carbon-based high-performance devices.

3. Conclusion

In summary, we have developed a technique to obtain ultrahigh-purity long s-SWCNTs by sonication control and multiple iterative separations with gel chromatography. The implementation of multiple low-power short-duration sonication cycles significantly reduced defect levels while preserving the proportion of long SWCNTs without compromising yields. The iterative separation process enhanced the purity of s-SWCNTs to the extent that signals of m-SWCNTs were completely eliminated in both optical absorption and Raman spectra. Electrical performance measurements combined with Monte Carlo simulations revealed that the purity of the sorted s-SWCNTs exceeded 99.9999%, marking the highest reported purity in aqueous systems. TFTs based on the s-SWCNTs separated by our method exhibit superior electrical properties, including a high on-state conductance of 149 μS μm^{-1}, excellent mobility of 89.1 cm^{2}V^{-1}s^{-1} while remaining a high on/off ratio of 10^5. This work establishes a robust material foundation for the development of large-scale, high-performance SWCNT-based devices. Gel chromatography, similar to other surfactant-based separation techniques such as ATPE and DGU, relies on the dispersion of SWCNTs in aqueous solutions by surfactants and the selective adsorption of these surfactants onto the surfaces of m- and s-SWCNTs, resulting in their separation. Our present findings thus provide a valuable reference for the separation of ultra-pure, long s-SWCNTs using ATPE and DGU separation methods.

4. Experimental Section

The Effects of Sonication on the Defects, Length, and Dispersion Degree of SWCNTs: Arc-discharged (AD) single-wall carbon nanotubes (SWCNTs) with diameters ranging from 1.3 to 2.3 nm (Sigma-Aldrich, Lot # MKBW5848V) were utilized as pristine materials. A quantity of 12 mg of AD-SWCNTs was dispersed in 20 mL of aqueous solutions containing 0.5 wt.% sodium cholate (SC, 99.0%, Sigma–Aldrich) using a tip ultrasonic homogenizer (Sonifire 450D, Branson) at a power density of 30 W cm^{-2} for varying durations (10, 30 min, 1, 2, 3, 4, 6, and 8 h). To prevent thermal damage, the system was maintained in a water bath at 15 °C. Following sonication, the dispersion underwent ultracentrifugation (S50A, CS150FNX, Hitachi) at 210 000 g for 1 h, after which the upper 80% of the supernatant was collected for further processing. The ultracentrifuged samples, corresponding to different sonication durations, were adjusted to a uniform SWCNT concentration by dilution. Sodium dodecyl sulfate (SDS, 99.0%, Sigma-Aldrich) and deionized water were added to establish a mixed surfactant system comprising 0.6 wt.% SDS and 0.1 wt.% SC. To ensure consistent SWCNT loading, appropriate volumes of the surfactant solution (0.6 wt.% SDS and 0.1 wt.% SC) were added to the sonicated SWCNT suspensions, maintaining a constant SWCNT concentration. Subsequently, 10 mL of the mixed SWCNT solution was loaded onto a gel column filled with 5 mL of Sephacryl S-200 HR gel beads (GE Healthcare). Unadsorbed SWCNTs were eluted with a cosurfactant solution of 0.6 wt.% SDS + 0.1 wt.% SC, while adsorbed SWCNTs were subsequently eluted with a 0.5 wt.% SC solution.

The Effects of Ultracentrifugation Durations on the Dispersion Degree of SWCNTs: 12 mg of AD-SWCNTs was dispersed in 20 mL of aqueous solutions of 0.5 wt.% SC using a tip ultrasonic homogenizer (Sonifire 450D, Branson) at a power density of 30 W cm^{-2} for 10 min. Subsequently, the solution underwent ultracentrifugation at varying time intervals (15, 30, 45 min, 1, 1.5, 2, and 3 h). The upper 80% of the supernatant was collected for the separation of m-/s-SWCNT to evaluate the dispersion degree of SWCNTs.

The Multiple Iterative Separations: The sonication and ultracentrifugation procedures were conducted as previously described. Specifically, the sonication duration was set to 10 min, while the ultracentrifugation period was established at 1 h. Subsequently, 225 mL of a dispersed SWCNT solution (comprising 0.6 wt.% SDS and 0.1 wt.% SC) was introduced into a pre-equilibrated gel column (70 mL). Unadsorbed SWCNTs were eluted using a cosurfactant of 0.6 wt.% SDS and 0.1 wt.% SC solution, whereas adsorbed SWCNTs were subsequently eluted with a 0.5 wt.% SC solution. The collected adsorbed SWCNT solution underwent ultracentrifugation at 210 000 g for 3 h to precipitate the SWCNTs. Following that, the SWCNT precipitate was redispersed in an aqueous solution of 0.6 wt.% SDS and 0.1 wt.% SC solution via sonication at a power density of 6 W cm^{-2} for 1 min per 20 mL. Finally, the re-dispersed SWCNT solution was subjected to ultracentrifugation at 210 000 g for 20 min to remove impurities. This iterative separation process was repeated similarly to the initial round.

Characterization of SWCNTs: Optical absorption spectra were recorded in the wavelength range of 200 to 1400 nm using a UV–vis–NIR spectrophotometer (UV-3600, Shimadzu). Raman spectra were acquired with a HORIBA LabRAM HR Evolution system, utilizing an excitation wavelength of 785 nm, and with a Princeton Instruments SpectraPro HRS-500 system, employing excitation wavelengths of 532 and 633 nm. The power of the laser was set to 10 mW. The morphological characteristics of the deposited SWCNT films were examined using atomic force microscopy (AFM, MultiMode 8, Bruker), and scanning electron microscopy (SEM, S-5200, Hitachi). The residual surfactants on the surface of s-SWCNTs were analyzed using a transmission electron microscope (TEM, JEM-ARM200F, JEOL).

The Fabrication and Characterization of SWCNT TFTs: The sorted s-SWCNTs were deposited on SiO_2/Si substrates utilizing the previously reported $NaHCO_3$ tuning method.[67] Specifically, the cleaned SiO_2/Si substrates underwent amination by immersion in a 0.1% PLL aqueous solution (Sigma–Aldrich) for 15 min. Subsequently, the amine-functionalized substrates were immersed in the prepared SWCNT solution containing 0.05 M $NaHCO_3$ to prepare films. Prior to TFT construction, the surfactant on the deposited s-SWCNTs was removed via a combination of thermal treatment and rinsing processes. Specifically, the samples were annealed under an Ar atmosphere at 300 °C for 30 min, followed by annealing at 500 °C for 45 min. Subsequently, the samples were rinsed with diluted HCl (volume ratio: $HCl/H_2O = 1:10$) to eliminate residual impurities, and then further rinsed with deionized water before being dried using Ar gas.[38] For back-gated TFTs, the channel area was defined as 400 nm in length and 50 µm in width via electron beam lithography (EBL, Raith 150, Raith). Ti/Pd stack films of 0.5/40 nm thickness were deposited via thermal evaporation (TE) using equipment from SKY Technology to form the source and drain electrodes. Heavily doped silicon functioned as gate electrodes. Reactive ion etching (RIE) (Plasmalab 80 Plus, Oxford Instruments) was employed to remove SWCNTs outside the active area. For top-gated TFTs, the fabrication process was similar to that of back-gated TFTs. The channel area was defined as 400 nm in length and 3.5 µm in width via EBL. An HfO_2 film of 10 nm thickness was deposited via atomic layer deposition (Savannah-100, Cambridge NanoTech). Ti/Pd stack films of 0.5/40 nm thickness were deposited as the electrodes. Electrical performance measurements of the TFTs were conducted using a semiconductor analyzer (4200A-SCS, Keithley) within a probe station (Lakeshore TTPX).

Supporting Information

Supporting Information is available from the Wiley Online Library or from the author.

Acknowledgements

This work was financially supported by the National Key Research and Development Program of China (Grant Nos. 2020YFA0714700 and 2024YFA1210602), the National Natural Science Foundation of China (Grant Nos. 51820105002, 11634014, 51872320, 52172060, and 12174086), the Strategic Priority Research Program of the Chinese Academy of Sciences (Grant No. XDB33030100), the Youth Innovation Promotion Association of CAS (Grant No. 2020005) and the Key Research and Development Program of Jiangsu Province (BK20232009).

Conflict of Interest

The authors declare no conflict of interest.

Data Availability Statement

The data that support the findings of this study are available in the supplementary material of this article.

Keywords

gel chromatography, high performance, long length, semiconducting carbon nanotubes, ultrahigh purity

Received: March 25, 2025
Revised: May 10, 2025
Published online:

[1] T. Dürkop, S. A. Getty, E. Cobas, M. S. Fuhrer, *Nano Lett.* **2004**, *4*, 35.
[2] G. J. Brady, A. J. Way, N. S. Safron, H. T. Evensen, P. Gopalan, M. S. Arnold, *Sci. Adv.* **2016**, *2*, 1601240.
[3] P. Avouris, Z. Chen, V. Perebeinos, *Nat. Nanotechnol.* **2007**, *2*, 605.
[4] A. Javey, H. Kim, M. Brink, Q. Wang, A. Ural, J. Guo, P. McIntyre, P. McEuen, M. Lundstrom, H. Dai, *Nat. Mater.* **2002**, *1*, 241.
[5] A. Javey, J. Guo, Q. Wang, M. Lundstrom, H. Dai, *Nature* **2003**, *424*, 654.
[6] X. J. Zhou, J. Y. Park, S. M. Huang, J. Liu, P. L. McEuen, *Phys. Rev. Lett.* **2005**, *95*, 146805.
[7] S. M. Bachilo, M. S. Strano, C. Kittrell, R. H. Hauge, R. E. Smalley, R. B. Weisman, *Science* **2002**, *298*, 2361.
[8] G S. Tulevski, A D. Franklin, D. Frank, J M. Lobez, Q. Cao, H. Park, A. Afzali, S.-J. Han, J B. Hannon, W. Haensch, *ACS Nano* **2014**, *8*, 8730.
[9] L. M. Peng, Z. Y. Zhang, S. Wang, *Mater. Today* **2014**, *17*, 433.
[10] M. M. S. Aly, M. Y. Gao, G. Hills, C. S. Lee, G. Pitner, M. M. Shulaker, T. F. Wu, M. Asheghi, J. Bokor, F. Franchetti, K. E. Goodson, C. Kozyrakis, I. Markov, K. Olukotun, L. Pileggi, E. Pop, J. Rabaey, C. Ré, H. S. P. Wong, S. Mitra, *Computer* **2015**, *48*, 24.
[11] A. D. Franklin, *Nature* **2013**, *498*, 443.
[12] L. Ding, A. Tselev, J. Wang, D. Yuan, H. Chu, T P. McNicholas, Y. Li, J. Liu, *Nano Lett.* **2009**, *9*, 800.
[13] W. Zhou, S. Zhan, L. Ding, J. Liu, *J. Am. Chem. Soc.* **2012**, *134*, 14019.
[14] X. Qin, F. Peng, F. Yang, X. He, H. Huang, Da Luo, J. Yang, S. Wang, H. Liu, L. Peng, Y. Li, *Nano Lett.* **2014**, *14*, 512.
[15] J. Wang, X. Jin, Z. Liu, G. Yu, Q. Ji, H. Wei, J. Zhang, Ke Zhang, D. Li, Zi Yuan, J. Li, P. Liu, Y. Wu, Y. Wei, J. Wang, Q. Li, L. Zhang, J. Kong, S. Fan, K. Jiang, *Nat. Catal.* **2018**, *1*, 326.
[16] K. Yanagi, T. Iitsuka, S. Fujii, H. Kataura, *J. Phys. Chem. C* **2008**, *112*, 18889.
[17] C. M. Homenick, A. Rousina-Webb, F. Cheng, M. B. Jakubinek, P. R. L. Malenfant, B. Simard, *J. Phys. Chem. C* **2014**, *118*, 16156.
[18] M. Zheng, A. Jagota, E D. Semke, B A. Diner, R S. Mclean, S R. Lustig, R E. Richardson, N G. Tassi, *Nat. Mater.* **2003**, *2*, 338.
[19] M. Zheng, A. Jagota, M S. Strano, A P. Santos, P. Barone, S. G Chou, B A. Diner, M S. Dresselhaus, R S. Mclean, G. B Onoa, G G. Samsonidze, E D. Semke, M. Usrey, D J. Walls, *Science* **2003**, *302*, 1545.
[20] T. Tanaka, Y. Urabe, D. Nishide, H. Kataura, *Appl. Phys. Express* **2009**, *2*, 125002.
[21] G. S. Tulevski, A. D. Franklin, A. Afzali, *ACS Nano* **2013**, *7*, 2971.
[22] D. Yang, J. Hu, H. Liu, S. Li, W. Su, Q. Li, N. Zhou, Y. Wang, W. Zhou, S. Xie, H. Kataura, *Adv. Funct. Mater.* **2017**, *27*, 1700278.
[23] J. Cui, W. Su, D. Yang, S. Li, X. Wei, N. Zhou, W. Zhou, S. Xie, H. Kataura, H. Liu, *ACS Appl. Nano Mater.* **2019**, *2*, 343.
[24] C. Y. Khripin, J. A. Fagan, M. Zheng, *J. Am. Chem. Soc.* **2013**, *135*, 6822.
[25] H. Gui, J. K. Streit, J. A. Fagan, A. R. Hight Walker, C. Zhou, M. Zheng, *Nano Lett.* **2015**, *15*, 1642.
[26] L. Wei, B. S. Flavel, W. S. Li, R. Krupke, Y. Chen, *Nanoscale* **2017**, *9*, 11640.
[27] H. W. Lee, Y. Yoon, S. Park, J. H. Oh, S. Hong, L S. Liyanage, H. Wang, S. Morishita, N. Patil, Y. J. Park, J. J. Park, A. Spakowitz, G. Galli, F. Gygi, P H.-S. Wong, J B.-H. Tok, J. M. Kim, Z. Bao, *Nat. Commun.* **2011**, *2*, 541.
[28] W. Gomulya, G. D. Costanzo, E. J. F. de Carvalho, S. Z. Bisri, V. Derenskyi, M. Fritsch, N. Fröhlich, S. Allard, P. Gordiichuk, A. Herrmann, S. J. Marrink, M. C. dos Santos, U. Scherf, M. A. Loi, *Adv. Mater.* **2013**, *25*, 2948.
[29] J. Gu, J. Han, D. Liu, X. Yu, L. Kang, S. Qiu, H. Jin, H. Li, Q. Li, J. Zhang, *Small* **2016**, *12*, 4993.
[30] T. Lei, X. Chen, G. Pitner, H. S. P. Wong, Z. Bao, *J. Am. Chem. Soc.* **2016**, *138*, 802.

[31] L. Liu, J. Han, L. Xu, J. Zhou, C. Zhao, S. Ding, H. Shi, M. Xiao, Li Ding, Ze Ma, C. Jin, Z. Zhang, L.-M. Peng, *Science* **2020**, *368*, 850.
[32] L. Cao, Y. Li, Ye Liu, J. Zhao, Z. Nan, W. Xiao, S. Qiu, L. Kang, H. Jin, Q. Li, *ACS Nano* **2024**, *18*, 3783.
[33] W. Z. Wang, W. F. Li, X. Y. Pan, C. M. Li, L.-J. Li, Yu G Mu, J. A. Rogers, M B. Chan-Park, *Adv. Funct. Mater.* **2011**, *21*, 1643.
[34] H. P. Liu, D. Nishide, T. Tanaka, H. Kataura, *Nat. Commun.* **2011**, *2*, 309.
[35] H. P. Liu, T. Tanaka, Y. Urabe, H. Kataura, *Nano Lett.* **2013**, *13*, 1996.
[36] D. Yang, L. Li, X. Wei, Y. Wang, W. Zhou, H. Kataura, S. Xie, H. Liu, *Sci. Adv.* **2021**, *7*, abe0084.
[37] D. Yang, L. Li, X. Li, W. Xi, Y. Zhang, Y. Liu, X. Wei, W. Zhou, F. Wei, S. Xie, H. Liu, *Nat. Commun.* **2023**, *14*, 2491.
[38] X. Li, W. Wang, H. Xiao, Y. Zhang, C. Liu, S. Li, L. Li, W. Su, Y. Wang, X. Wei, Y. Li, H. Liu, W. Zhou, H. Liu, *Carbon* **2024**, *218*, 118750.
[39] M S. Strano, V C. Moore, M K. Miller, M J. Allen, E H. Haroz, C. Kittrell, R H. Hauge, R. E. Smalley, *J. Nanosci. Nanotechnol.* **2003**, *3*, 81.
[40] A. J. Blanch, C. E. Lenehan, J. S. Quinton, *Carbon* **2011**, *49*, 5213.
[41] A. Lucas, C. Zakri, M. Maugey, M. Pasquali, P. van der Schoot, P. Poulin, *J. Phys. Chem. C* **2009**, *113*, 20599.
[42] P. Vichchulada, M. A. Cauble, E. A. Abdi, E. I. Obi, Q. Zhang, M. D. Lay, *J. Phys. Chem. C* **2010**, *114*, 12490.
[43] G. Pagani, M. J. Green, P. Poulin, M. Pasquali, *Proc. Natl. Acad. Sci. USA* **2012**, *109*, 11599.
[44] J. Stegen, *J. Chem. Phys.* **2014**, *140*, 244908.
[45] Y. Kuwahara, F. Nihey, S. Ohmori, T. Saito, *Carbon* **2015**, *91*, 370.
[46] W. Su, X. Li, L. Li, D. Yang, F. Wang, X. Wei, W. Zhou, H. Kataura, S. Xie, H. Liu, *Nat. Commun.* **2023**, *14*, 1672.
[47] M. F. Islam, E. Rojas, D. M. Bergey, A. T. Johnson, A. G. Yodh, *Nano Lett.* **2003**, *3*, 269.
[48] C. Wang, J. Zhang, C. Zhou, *ACS Nano* **2010**, *4*, 7123.
[49] V K. Sangwan, R. P. Ortiz, J M. P. Alaboson, J D. Emery, M J. Bedzyk, L J. Lauhon, T J. Marks, M. C. Hersam, *ACS Nano* **2012**, *6*, 7480.
[50] H. Li, G. Gordeev, O. Garrity, N. A. Peyyety, P. B. Selvasundaram, S. Dehm, R. Krupke, S. Cambré, W. Wenseleers, S. Reich, M. Zheng, J A. Fagan, B S. Flavel, *ACS Nano* **2020**, *14*, 948.
[51] Y. Miyata, K. Shiozawa, Y. Asada, Y. Ohno, R. Kitaura, T. Mizutani, H. Shinohara, *Nano Res.* **2011**, *4*, 963.
[52] C. Wang, J. L. Zhang, K. M. Ryu, A. Badmaev, L. G. De Arco, C. W. Zhou, *Nano Lett.* **2009**, *9*, 4285.
[53] Y. Li, M. Zheng, J. Yao, W. Gong, Y. Li, J. Tang, S. Feng, R. Han, Q. Sui, S. Qiu, L. Kang, H. Jin, D. Sun, Q. Li, *Adv. Funct. Mater.* **2022**, *32*, 2107119.
[54] S. Böttger, S. Hermann, S. E. Schulz, T. Gessner, *Nanotechnology* **2016**, *27*, 435203.
[55] J. Yao, Y. Li, Y. Li, Q. Sui, H. Wen, L. Cao, P. Cao, L. Kang, J. Tang, H. Jin, S. Qiu, Q. Li, *Carbon* **2021**, *184*, 764.
[56] F. Hennrich, W. S. Li, R. Fischer, S. Lebedkin, R. Krupke, M. M. Kappes, *ACS Nano* **2016**, *10*, 1888.
[57] J. L. Zhang, H. Gui, B. L. Liu, J. Liu, C. W. Zhou, *Nano Res.* **2013**, *6*, 906.
[58] B. Thendie, H. Omachi, J. Hirotani, Y. Ohno, Y. Miyata, H. Shinohara, *Jpn. J. Appl. Phys.* **2017**, *56*, 065102.
[59] D. Yang, K. Hwang, Y-Ju Kim, Y. Kim, Y. Moon, N. Han, M. Lee, S.-H. Lee, D-Yu Kim, *Carbon* **2023**, *206*, 351.
[60] C. Y. Cao, J. B. Andrews, A. Kumar, A. D. Franklin, *ACS Nano* **2016**, *10*, 5221.
[61] G. Dong, J. Zhao, L. Shen, J. Xia, Hu Meng, W. Yu, Qi Huang, H. Han, X. Liang, L. Peng, *Nano Res.* **2018**, *11*, 4356.
[62] J. Xia, G. Dong, B. Tian, Q. Yan, H. Zhang, X. Liang, L. Peng, *Nanoscale* **2016**, *8*, 9988.
[63] X. Zeng, D. H. Yang, H. P. Liu, N. G. Zhou, Y. C. Wang, W. Y. Zhou, S. S. Xie, H. Kataura, *Adv. Mater. Interfaces* **2018**, *5*, 1700727.
[64] G. E. Pike, C. H. Seager, *Phys. Rev. B* **1974**, *10*, 1421.
[65] I. Balberg, N. Binenbaum, C. H. Anderson, *Phys. Rev. Lett.* **1983**, *51*, 1605.
[66] J. Heitz, Y. Leroy, L. Hebrard, C. Lallement, *Nanotechnology* **2011**, *22*, 345703.
[67] W. Su, D. Yang, J. Cui, F. Wang, X. Wei, W. Zhou, H. Kataura, S. Xie, H. Liu, *Carbon* **2020**, *163*, 370.
[68] J. Ding, Z. Li, J. Lefebvre, F. Cheng, G. Dubey, S. Zou, P. Finnie, A. Hrdina, L. Scoles, G P. Lopinski, C T. Kingston, B. Simard, P R. L. Malenfant, *Nanoscale* **2014**, *6*, 2328.
[69] H. Kataura, Y. Kumazawa, Y. Maniwa, I. Umezu, S. Suzuki, Y. Ohtsuka, Y. Achiba, *Synth. Met.* **1999**, *103*, 2555.
[70] R. B. Weisman, S. M. Bachilo, *Nano Lett.* **2003**, *3*, 1235.
[71] S. Ling, X. Wei, X. Luo, X. Li, S. Li, F. Xiong, W. Zhou, S. Xie, H. Liu, *Small* **2024**, *20*, 2400303.
[72] S. Attal, R. Thiruvengadathan, O. Regev, *Anal. Chem.* **2006**, *78*, 8098.
[73] IsoNanotubes-S of NanoIntegris Technologies, Inc., https://nanointegris.com/ (accessed: May 2025).
[74] High-purity s-SWCNT solution of Suzhou Carbon Semiconductor Technology Co., Ltd., http://www.cs-tec.com.cn (accessed: May 2025).
[75] H. Y. Teah, T. Sato, K. Namiki, M. Asaka, K. S. Feng, S. Noda, *ACS Sustainable Chem. Eng.* **2020**, *8*, 1730.
[76] P. Lamberti, S. A. Mousavi, G. Spinelli, V. Tucci, V. Wagner, *IEEE Trans. Nanotechnol.* **2014**, *13*, 795.
[77] S. Tripathy, B. Bose, P. P. Chakrabarti, T. K. Bhattacharyya, *IEEE Trans. Electron Devices* **2020**, *67*, 5676.
[78] M. Bockrath, W. Liang, D. Bozovic, J H. Hafner, C M. Lieber, M. Tinkham, H. Park, *Science* **2001**, *291*, 283.
[79] C. Gómez-Navarro, P. J. De Pablo, J. Gómez-Herrero, B. Biel, F. J. Garcia-Vidal, A. Rubio, F. Flores, *Nat. Mater.* **2005**, *4*, 534.